



Hidden in Plain Sight II: Characterizing the luminous companion to κ Velorum with VLTI/GRAVITY

D. M. ROWAN ^{1,*}, S. KRAUS,² AND TODD A. THOMPSON ^{3,4,5}

¹Department of Astronomy, University of California, Berkeley, CA 94720, USA

²Astrophysics Group, Department of Physics & Astronomy, University of Exeter, Stocker Road, Exeter EX4 4QL, UK

³Department of Astronomy, The Ohio State University, 140 West 18th Avenue, Columbus, OH, 43210, USA

⁴Center for Cosmology and Astroparticle Physics, The Ohio State University, 191 W. Woodruff Avenue, Columbus, OH, 43210, USA

⁵Department of Physics, The Ohio State University, Columbus, Ohio, 43210, USA

ABSTRACT

κ Vel (Markeb, HD 81188) is one of the brightest stars in the Southern sky and has long been known to be a single-lined spectroscopic binary. The binary mass function is large, $f(M) = 1.15 M_{\odot}$, suggesting that the bright ($V = 2.5$) B2IV star may host a dark, compact object companion. We use VLTI GRAVITY observations to definitively test this possibility by directly resolving the binary. We detect a main sequence B star companion and rule out the compact object scenario. By combining the relative astrometric orbit and archival radial velocities, we report an updated precise characterization of the orbit (period $P = 116.795 \pm 0.002$ d, eccentricity $e = 0.1764 \pm 0.0004$, inclination $i = 74.04 \pm 0.01^{\circ}$) and estimate the masses of the B stars. Using the original Hipparcos parallax measurement $\varpi = 6.05 \pm 0.48$ mas, we find $M_1 = 10_{-2}^{+4} M_{\odot}$ and $M_2 = 6.9 \pm 1.0 M_{\odot}$. The uncertainties on the masses are primarily driven by the uncertain parallax, which we find is likely biased by the orbital motion. We use an archival UVES spectrum and MIST evolutionary tracks to refine our mass estimates. Finally, we discuss how interferometry and high-contrast imaging may be used to characterize other candidate star+compact object binaries, including those that will be discovered with *Gaia* DR4, as part of a larger effort to uncover the hidden population of black holes in the Milky Way.

Keywords: Binary stars(154) — Compact objects(288) — Direct imaging(387)

1. INTRODUCTION

The majority of the observed black holes and neutron stars in the Milky Way have been detected in X-ray binary systems (Corral-Santana et al. 2016). While compact object masses can sometimes be measured dynamically in these systems, either by inferring the orbital inclination from the accretion disk properties (e.g., Torres et al. 2020) or by modeling ellipsoidal modulations (e.g., Orosz et al. 2001), many of the transient BH candidates have no mass measurements (e.g., Russell et al. 2022). Since X-ray binaries are expected to undergo at least one episode of binary interaction and mass transfer (Kalogera & Webbink 1996; Tauris & van den Heuvel 2006), the observed compact object mass distribution from X-ray binaries may present a biased view of the intrinsic distribution.

Outside of the Galaxy, gravitational waves have been used to detect > 150 compact object binary mergers (The LIGO Scientific Collaboration et al. 2025b). While these targets provide powerful constraints on the mass distribution of black holes (The LIGO Scientific Collaboration et al. 2025a), these

rare extragalactic systems are also the products of complex binary interactions that result in a coalescence. The majority of the observed gravitational wave sources are also more massive than typical X-ray binaries, since more massive black hole mergers have a larger characteristic strain.

In recent years, there has been an increased effort to uncover the hidden population of dormant black holes in the Milky Way. Isolated black holes can only be detected via microlensing (Lam et al. 2022; Lam & Lu 2023). While there is currently only one strong candidate, the Vera C. Rubin Legacy Survey of Space and Time and the Roman Space Telescope are expected to detect $\gtrsim 30$ isolated black holes (Abrams et al. 2025; Lam et al. 2023). Multiple observational methods can be used to detect and characterize black holes in wide binaries with luminous companions. Three black holes have been detected using *Gaia* astrometry (El-Badry et al. 2023a,b; Chakrabarti et al. 2023; Tanikawa et al. 2023), including *Gaia*-BH3, a red giant star in the Milky Way halo with a $33 M_{\odot}$ black hole in an 11.9 year binary orbit (Gaia Collaboration et al. 2024). Spectroscopic surveys have also been applied to search for candidates (e.g., Giesers et al. 2018; Shenar et al. 2022; Mahy et al. 2022), but the unknown

* NHFP Hubble Fellow

orbital inclination means that only a minimum black hole mass can be measured. At short orbital periods ($P \lesssim 10$ days for main sequence companions), ellipsoidal modulations can be used to measure the orbital inclination (Morris & Naftilan 1993), but no strong candidates have been discovered starting from photometric variability (Rowan et al. 2021; Green et al. 2025).

Regardless of whether a black hole candidate is detected with astrometry, spectroscopy, or photometry, confirming a black hole effectively means ruling out any type of luminous companion. For some systems, like the $33 M_\odot$ black hole in *Gaia* BH3, the spectral energy distribution can easily exclude a massive main sequence star or an equal-mass binary of two $16.5 M_\odot$ stars. For lower-mass black holes, spectral disentangling can be help to distinguish compact objects from false positives, such as rapidly rotating subgiants (e.g., El-Badry et al. 2022; Jayasinghe et al. 2022). However, if we can directly resolve a candidate system with high-contrast imaging or interferometry, we can detect or rule out luminous companions with a single observation (e.g., Frost et al. 2022).

If we observe a stellar binary, the direct imaging observations will resolve the two stars and help constrain the three-dimensional orbit. If we instead resolve a non-interacting black hole binary, we expect to observe a single point source. The combination of RVs and astrometry can therefore be used to unambiguously detect and characterize non-interacting black hole binary systems. In Rowan et al. (2025), we performed a pilot study to explore the feasibility of this method using SHARK-VIS (Pedichini et al. 2022; Pedichini et al. 2024) on the Large Binocular Telescope (Hill et al. 2010). We ruled out black holes for three of the four systems observed, and showed that two of the binaries selected are likely hierarchical triples. Since the SHARK-VIS observations only require ~ 10 min of on-sky observing time, direct imaging can be used to rapidly vet black hole candidates in long period orbits more efficiently than high-resolution spectroscopic follow-up.

Here, we use VLTI/GRAVITY to observe κ Velorum (hereafter κ Vel), a bright ($V = 2.5$), single-lined spectroscopic binary with an RV orbit that indicates a large, massive companion. Section §2 describes how we selected this target as a potential black hole candidate. Section §3 reports the VLTI/GRAVITY observations and the describes the data reduction. We unambiguously detect a second star in the VLTI GRAVITY observations and rule out a black hole. We then characterize the stellar binary by simultaneously fitting the archival RVs with the relative astrometry in Section §4, model an archival high resolution spectrum (Section §5), and make comparisons to evolutionary tracks of massive stars (Section §6). Finally, we discuss the prospects for observing other high-mass function single-lined spectroscopic binaries with interferometry and direct imaging in Section §7.

2. TARGET SELECTION

We selected targets following the procedure outlined in Rowan et al. (2025). In short, we started from two large catalogs of spectroscopic binaries, the Ninth Catalog of Spectroscopic Binary Orbits (Pourbaix et al. 2004, hereafter SB9) and single-lined spectroscopic binaries from the *Gaia* DR3 non-single stars catalog (Gaia Collaboration et al. 2023; Gosset et al. 2024, hereafter *Gaia* SB1). We used the astrophysical parameter estimates from StarHorse (Anders et al. 2022) to estimate the mass of the photometric primaries, and determined the minimum companion masses and maximum projected orbital separations based on the archival RV orbits. Figure 1 shows the maximum projected orbital separations and minimum companion mass measurements.

We identified κ Vel (HD 81188, HIP 45941) as having a large minimum companion mass and an angular separation accessible with VLTI GRAVITY. With an apparent magnitude of $V = 2.5$, κ Vel is one of the brightest stars in the Southern sky and has been targeted as part of a number of surveys, but the secondary has not previously been characterized. κ Vel has been most commonly observed as part of interstellar medium absorption line studies (e.g., Crawford 1991; Fruscione et al. 1994; Jenniskens et al. 1997; Crawford 2002; Smith et al. 2013; Cox et al. 2017). κ Vel was first identified as a binary candidate by Wright (1905) and the orbit was characterized by Curtis (1907) as part of the D.O. Mills Expedition from Lick Observatory to the Southern Hemisphere. Five additional measurements taken by Buscombe & Morris (1960) confirmed the RV variability and orbit. Table 1 lists the archival measurements. We assume an RV uncertainty of 5 km/s for the Curtis (1907) measurements since measurement errors were not reported. Chini et al. (2012) also measured four RVs of κ Vel as part of a spectroscopic surveys of massive stars. They classify the system as an SB1, but the individual RV measurements or spectra are not available. κ Vel is included in the SB9 catalog with an orbital period of $P = 116.65$ days, $K_1 = 46.5$ km/s, and a binary mass function $f(M) = 1.15 M_\odot$, where

$$f(M) = \frac{PK^3}{2\pi G} (1 - e^2)^{3/2} = \frac{M_2^3 \sin^3 i}{(M_1 + M_2)^2}, \quad (1)$$

M_1 is the photometric primary mass, M_2 is the companion mass, i is the orbital inclination, and e is the orbital eccentricity. The photometric primary is spectroscopically characterized as a B2IV star (Levato 1975), which roughly corresponds to a primary mass of $\sim 7\text{--}10 M_\odot$ (Pecaut & Mamajek 2013). Based on the RV orbit, even if the primary is $7 M_\odot$ and the orbit is edge-on, the companion must be $> 5.7 M_\odot$ (Figure 2). Because of the large minimum companion mass, Trimble & Thorne (1969) included κ Vel in their catalog of binaries that could host compact object companions. The companion could be another massive star, a compact object, or an in-

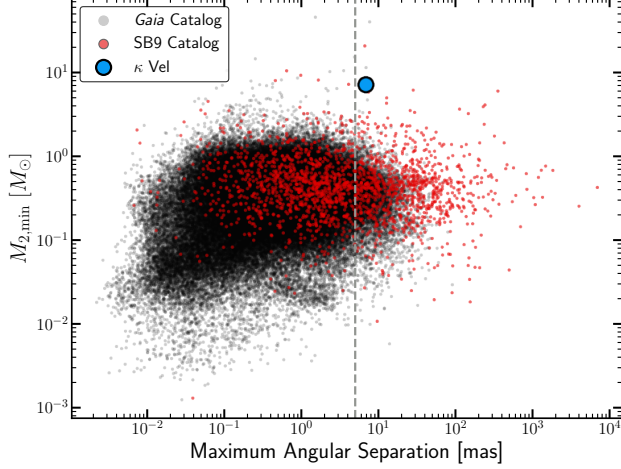


Figure 1. Minimum companion masses, $M_{2,\min}$, and maximum projected angular separation for binaries in the *Gaia* SBIs and SB9 catalogs. κ Vel is marked in blue. The vertical line marks the projected angular separation resolvable with VLTI GRAVITY.

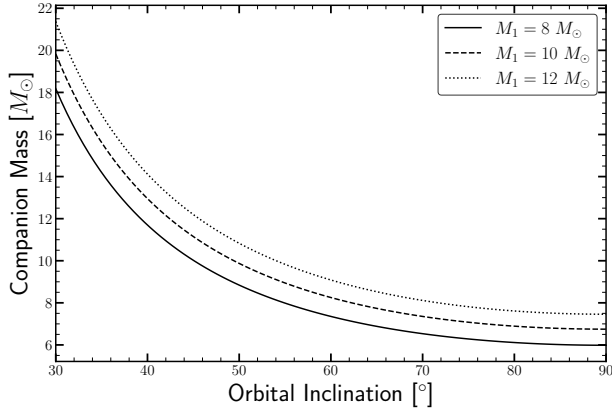


Figure 2. Companion mass, M_2 , as a function of the orbital inclination for different values of the primary mass, M_1 . Even if the primary mass is $8 M_{\odot}$, the companion must be $\gtrsim 6 M_{\odot}$.

ner binary of two lower mass stars. The maximum projected orbital separation is > 7.0 mas (Figure 1), making this a suitable target for VLTI direct imaging observations to test these possibilities.

3. VLTI/GRAVITY OBSERVATIONS

We observed κ Vel at nine epochs between December 2024 and February 2025 using the European Southern Observatory’s Very Large Telescope Interferometer (VLTI) as part of observing program 114.274C (PI: Thompson). The GRAVITY instrument (GRAVITY Collaboration et al. 2017) was used to combine the four auxiliary telescopes (ATs) that were in the large (A0-G1-J2-K0) and extended (A0-B5-J2-J6) array configuration, resulting in maximum baselines D_{\max} up to 129.3 and 201.5 meters, respectively. The observations

Table 1. Archival RV measurements of κ Vel from Curtis (1907) and Buscombe & Morris (1960). Since Curtis (1907) do not report RV uncertainties, we estimate a conservative RV uncertainty of 5 km/s. We also include our RV measurement from the UVES spectrum. We assign an RV uncertainty on the UVES spectrum of 2 km/s to account for the unknown systematic RV offset between the archival measurements and the UVES measurement.

JD $- 2.4165 \times 10^6$ [d]	RV [km/s]	σ_{RV} [km/s]	Reference
46.24	68.4	5.0	Curtis07
360.20	12.9	5.0	Curtis07
397.15	65.7	5.0	Curtis07
412.10	53.3	5.0	Curtis07
1087.35	58.6	5.0	Curtis07
1088.29	57.9	5.0	Curtis07
1090.33	58.5	5.0	Curtis07
1091.33	64.8	5.0	Curtis07
1097.29	65.8	5.0	Curtis07
1109.29	62.0	5.0	Curtis07
1154.04	-21.0	5.0	Curtis07
1155.06	-19.2	5.0	Curtis07
1158.07	-15.2	5.0	Curtis07
1159.05	-14.5	5.0	Curtis07
1186.09	33.8	5.0	Curtis07
1191.07	38.2	5.0	Curtis07
1192.06	43.2	5.0	Curtis07
1195.98	46.7	5.0	Curtis07
1201.00	52.7	5.0	Curtis07
1240.97	22.1	5.0	Curtis07
1245.96	0.3	5.0	Curtis07
1248.97	-7.6	5.0	Curtis07
1249.98	-8.8	5.0	Curtis07
1250.96	-13.3	5.0	Curtis07
1252.96	-19.2	5.0	Curtis07
1257.95	-29.0	5.0	Curtis07
1258.96	-24.5	5.0	Curtis07
18321.98	-21.0	4.5	Buscombe60
19736.10	12.0	3.2	Buscombe60
19760.96	39.0	7.1	Buscombe60
20472.10	45.0	4.9	Buscombe60
20501.99	38.0	6.2	Buscombe60
41361.55	26.6	2.0	UVES

were conducted in the K -band (2.0 – $2.45 \mu\text{m}$), resulting in an effective angular resolution of $\lambda/2D_{\max} = 1.0$ milliarcseconds (mas). The GRAVITY science combiner spectrograph was configured for medium-spectral resolution (MR, $R = \lambda/\Delta\lambda = 500$) for the first five observations to achieve the highest signal-to-noise and the lowest companion detection limits. From these initial observations, it became clear that the

system is a relatively low-contrast binary, so we switched to GRAVITY's high-spectral resolution mode (HR, $R = 4000$) for the last three observations. We observed calibrator stars with known diameters that were observed immediately after the science star and used to calibrate instrumental and atmospheric effects. The observing dates, detector integration times (DITs), and choice of calibrator for each night are listed in Table 2. We used the public GRAVITY pipeline, version 1.7.0 to derive from each data set six calibrated visibilities and four closure phases. Given that the observation used a single calibrator per night, we applied a minimum squared visibility error of 0.02 and a minimum closure phase error of 0.5° in order to achieve a realistic representation of measurement uncertainties.

3.1. Astrometry model-fitting

The visibility and closure phase data shows strong sinusoidal modulations that are indicative of a close binary system. In order to quantify the binary star parameters, we fit geometric models with the PMOIRE modeling software (Mérand 2022). The free parameters are the relative separation vector of the two stars measured from the primary to the secondary (dRA, dDEC) and their K -band flux ratio ($\epsilon = f_2/f_1$). The stars are found to be unresolved, so we fixed the uniform-disk diameters in the fit to 0.1 mas. For the error estimation, we bootstrap over the individual measurements that were taken during each epoch. The derived astrometry is reported in Table 3.

4. ORBIT FITTING

We can constrain the binary orbit of κ Vel by combining the archival RVs and the relative astrometry. Given an additional measurement of the parallax, the individual component masses can be determined.

We simultaneously model the RVs and relative astrometry with Markov Chain Monte Carlo (MCMC) with *emcee* (Foreman-Mackey et al. 2013). We sample over six orbital parameters: the period, P , the periastron time, T_0 , the orbital inclination, i , the longitude of the ascending node, Ω , the eccentricity, e , and the longitude of periastron, ω . We parameterize the latter two as $\sqrt{e} \cos \omega$ and $\sqrt{e} \sin \omega$ for computational efficiency. The angular size of the astrometric orbit is the ratio of the orbital semi-major axis to the distance, $a_0 = a/d$. We sample over the velocity-semi amplitude of the photometric primary, K_1 , and the system velocity, γ . We include an offset δ_{RV} between the Curtis (1907) and Buscombe & Morris (1960) RVs to account for systematic differences between the instruments. We use a Gaussian prior on δ_{RV} centered on zero with $\sigma = 1.5$ km/s. Since there is only one UVES spectrum, we do not fit for the potential RV offset between the Curtis (1907) RVs and the UVES spectrograph, and instead choose to inflate the measured UVES RV uncertainty (see Section §5).

Finally, we include two additional terms to account for potentially underestimated uncertainties. The stellar jitter term, s , accounts for stellar variability and underestimated RV uncertainties (Price-Whelan et al. 2017). To account for underestimated astrometric uncertainties, we also include a multiplicative term, s_{ast} , that scales the bootstrapped astrometric uncertainties.

The log-likelihood is the sum of the log-likelihoods for the RV and astrometric measurements,

$$\ln \mathcal{L} = \ln \mathcal{L}_{\text{RV}} + \ln \mathcal{L}_{\text{ast}}. \quad (2)$$

The log-likelihood for the radial velocity observations is

$$\ln \mathcal{L}_{\text{RV}} = -\frac{1}{2} \sum_i \left[\frac{(\text{RV}_{\text{pred}}(t_i) - \text{RV}_i)^2}{\sigma_{\text{RV},i}^2 + s^2} + \ln(2\pi(\sigma_{\text{RV},i}^2 + s^2)) \right], \quad (3)$$

where $\text{RV}_{\text{pred}}(t_i)$ is calculated using the standard Keplerian orbit equations. The astrometric orbit term is

$$\ln \mathcal{L} = -\frac{1}{2} \sum_{i=1}^N \left[\frac{1}{s_{\text{ast}}^2} \mathbf{r}_i^T \mathbf{C}_i^{-1} \mathbf{r}_i + \ln |\mathbf{C}_i| \right] - 2N \ln s_{\text{ast}} - N \ln(2\pi), \quad (4)$$

where the residuals are

$$\mathbf{r}_i = \begin{bmatrix} x_i - x_{\text{pred}}(t_i, \theta) \\ y_i - y_{\text{pred}}(t_i, \theta) \end{bmatrix}, \quad (5)$$

and \mathbf{C}_i are the covariance matrices for each measurement. The astrometric orbit model positions $x_{\text{pred}}(t_i)$ and $y_{\text{pred}}(t_i)$ are

$$\begin{aligned} x_{\text{pred}}(t) &= x_{\text{cm}} - A(\cos E - e) - F(1 - e^2)^{1/2} \sin E(t) \\ y_{\text{pred}}(t) &= y_{\text{cm}} - B(\cos E - e) - G(1 - e^2)^{1/2} \sin E(t), \end{aligned} \quad (6)$$

where E is the eccentric anomaly, and x_{cm} and y_{cm} are the center-of-mass of the orbit. Since we are modeling the orbit in the frame of the photometric primary, $x_{\text{cm}} = y_{\text{cm}} = 0$. The coefficients A , B , F , and G are the Thiele-Innes elements computed from the standard Campbell orbital elements:

$$\begin{aligned} A &= a_0 (\cos \Omega \cos \omega - \cos i \sin \Omega \sin \omega) \\ B &= a_0 (\sin \Omega \cos \omega + \cos i \cos \Omega \sin \omega) \\ F &= a_0 (-\cos \Omega \sin \omega - \cos i \sin \Omega \cos \omega) \\ G &= a_0 (-\sin \Omega \sin \omega + \cos i \cos \Omega \cos \omega) \end{aligned} \quad (7)$$

We use 20 walkers and run the chains for 500,000 iterations. We visually inspect the walker distributions and discard the first 100,000 iterations as burn-in. We find that the Gelman-Rubin statistic is $\hat{R} < 1.01$ and the effective sample size is

Table 2. VLTI GRAVITY observation log. The dates are given for the start of the night. The calibrator uniform-disk (UD) diameters are estimated with the JMMC SearchCal tool (Chelli et al. 2016).

Date	MJD	Telescope	Spectral	DIT	Calibrator	Calibrator diameter
(UT)		configuration	setup	[s]		[mas]
2024-12-25	60670.24654	A0-G1-J2-K0	MR	1	HD81720	0.834 ± 0.073
2024-12-28	60672.23178	A0-G1-J2-K0	MR	1	HD83465	0.766 ± 0.077
2025-01-03	60679.26416	A0-B5-J2-J6	MR	1	HD80093	0.720 ± 0.071
2025-01-08	60684.24311	A0-B5-J2-J6	MR	1	HD83465	0.766 ± 0.077
2025-02-08	60715.17032	A0-B5-J2-J6	MR	1	HD80765	0.827 ± 0.080
2025-02-18	60725.17185	A0-B5-J2-J6	HR	10	HD81720	0.834 ± 0.073
2025-02-21	60728.04764	A0-B5-J2-J6	HR	10	HD80093	0.720 ± 0.071
2025-02-22	60729.07190	A0-B5-J2-J6	HR	10	HD80765	0.827 ± 0.080
2025-02-28	60731.05039	A0-G1-J2-K0	HR	10	HD83465	0.766 ± 0.077

Table 3. Astrometry for κ Vel. The measurement uncertainties are estimated by bootstrapping over the individual measurements taken during each epoch (Section §3.1). ρ is the correlation coefficient between the dRA and dDEC measurements and f_2/f_1 is the flux ratio in the K -band.

Date	dRA	dDEC	ρ	f_2/f_1
(UT)	[mas]	[mas]		
2024-12-25	-0.956 ± 0.002	-3.737 ± 0.003	-0.33	0.28 ± 0.01
2024-12-28	-0.678 ± 0.003	-4.259 ± 0.003	-0.61	0.28 ± 0.01
2025-01-03	$+0.331 \pm 0.002$	-5.806 ± 0.002	-0.17	0.29 ± 0.01
2025-01-08	$+1.025 \pm 0.002$	-6.568 ± 0.001	-0.01	0.29 ± 0.01
2025-02-08	$+2.203 \pm 0.003$	-1.529 ± 0.003	-0.19	0.29 ± 0.01
2025-02-18	$+0.631 \pm 0.005$	$+2.756 \pm 0.004$	-0.22	0.29 ± 0.01
2025-02-21	$+0.081 \pm 0.001$	$+3.833 \pm 0.001$	-0.32	0.28 ± 0.01
2025-02-22	-0.122 ± 0.002	$+4.176 \pm 0.001$	+0.60	0.28 ± 0.01
2025-02-28	$+0.510 \pm 0.001$	$+4.781 \pm 0.002$	-0.50	0.28 ± 0.01

$> 10,000$ for all parameters, suggesting that the chains have converged. Figure 4 shows the corner plot of the MCMC posteriors and random samples of the orbit model compared to the VLTI astrometry observations and Figure 3 shows the resulting orbit model. Table 4 reports the median and 1σ uncertainties of the posteriors.

Given a parallax, ϖ , and associated uncertainty, σ_ϖ , the binary masses M_1 and M_2 can be solved for using Kepler’s third law. Figure 5 shows the mass posteriors using the original Hipparcos parallax $\varpi = 6.05 \pm 0.48$ mas (ESA 1997). The revised Hipparcos parallax, which primarily includes improvements to attitude reconstruction, is $\varpi = 5.7 \pm 0.3$ mas (van Leeuwen 2007). The revised Hipparcos astrometry is a

“stochastic” solution, rather than the standard five-parameter solution, which includes an additional “cosmic noise” astrometric noise term. Unfortunately, although κ Vel has been observed by *Gaia*, since it is $G = 2.5$ mag, it is likely saturated (Fabricius et al. 2021) and has no reported parallax.

Using the original Hipparcos parallax, we measure masses of $M_1 = 10^{+4}_{-2} M_\odot$ and $M_2 = 6.9 \pm 1.0 M_\odot$ for the photometric primary and secondary, respectively, consistent with a binary system made up of two B stars. If we instead use the revised Hipparcos parallax, the masses are $M_1 = 13^{+3}_{-2} M_\odot$ and $M_2 = 7.7^{+0.9}_{-0.8} M_\odot$. The mass uncertainties are dominated by the parallax measurement error.

The orbital motion of the binary system could also bias the measured parallax, adding additional uncertainty to the measured masses. Since the measured mass ratio, q , is not the same as the flux ratio, ϵ , the center-of-light, or photocenter, of the system orbits the barycenter with semi-major axis

$$\alpha = a \left(\frac{q}{1+q} - \frac{\epsilon}{1+\epsilon} \right) \quad (8)$$

The ratio between the projected angular size of the photocenter semi-major axis and the measured parallax quantifies the potential bias. For α in AU, this ratio is simply $\alpha \sin i$.

We must estimate the flux ratio of the system in the Hipparcos H_p filter to determine the parallax bias. For a given mass pair of M_1 and M_2 and metallicity, we interpolate the MIST evolutionary tracks (Dotter 2016; Choi et al. 2016) onto the same age grid, calculate the K -band flux as a function of stellar age, and use the observed flux ratio to estimate the system age. We use the H_p -band flux ratio at this system age to calculate $\alpha \sin i$. We find $\alpha \sin i \approx 0.22$, which indicates that the parallax can be biased by the binary motion by as much as 22%. Since the mass ratio depends on the parallax, this fractional bias does increase with increasing distance, but only at the percent level.

5. UVES SPECTRA

κ Vel was previously observed with VLT UVES as part of the ESO Diffuse Interstellar Bands Large Exploration Survey (EDIBLES, Cox et al. 2017, 194.C-0833). κ Vel was observed on 2017-04-18 in all four UVES cross-dispersers (CDs). The Phase 3 data product includes the combined spectra for 20 individual exposures in CD1 and CD2 and for 14 and 15 exposures in CD3 and CD4, respectively. While the purpose of the EDIBLES program was to characterize diffuse interstellar bands (DIBs), we can also use the UVES κ Vel spectrum to characterize the photometric primary of the binary. We start by continuum normalizing the CD2 spectrum with a cubic spline, which covers a wavelength range of 370–500nm. We mask the Balmer lines during continuum normalization. Our analysis only uses the CD2 observations given the density of spectral features and lack of telluric lines.

We construct a grid of synthetic B star spectra using TLUSTY model atmospheres from the precomputed BSTAR2006 grid (Lanz & Hubeny 2007). We compute synthetic spectra with Synspec using these model atmospheres (Hubeny & Lanz 2011). The grid is ranges from $15 \leq T_{\text{eff}} \leq 30$ kK with a step size of 1 kK and $2.5 \leq \log g \leq 4.5$ with a step size of 0.25. We generate the grid at three metallicities: $Z = Z_{\odot}/2$, Z_{\odot} , and $2Z_{\odot}$. The microturbulence is fixed at 2 km/s since hot stars ($T_{\text{eff}} \gtrsim 10,000$ K) are not expected to have large microturbulent velocities (Landstreet et al. 2009). The synthetic spectra are broadened to match the UVES resolution ($R \approx 71,000$) with a Gaussian kernel. For each synthetic spectrum, we use χ^2 minimization to determine the RV

Table 4. MCMC posteriors for the combined RV and astrometry orbit fit. We report the mass measurements for the two different Hipparcos parallax measurements.

Parameter	Value
a/d [mas]	7.272 ± 0.004
K_1 [km/s]	44.0 ± 1.0
P [d]	116.795 ± 0.002
T_0 [d]	73.1 ± 0.6
e	0.1761 ± 0.0004
ω [deg]	95.79 ± 0.07
Incl [deg]	74.03 ± 0.02
Ω [deg]	109.74 ± 0.03
γ [km/s]	21.8 ± 0.8
$\ln(s$ [km/s])	-5.0 ± 3.0
$\ln(s_{\text{ast}}$ [mas])	0.8 ± 0.2
δRV_0 [km/s]	1.0 ± 1.0
<hr/>	
	$\varpi = 6.05 \pm 0.48$ mas $\varpi = 5.7 \pm 0.3$ mas
M_1 [M_{\odot}]	10^{+4}_{-2} 13^{+3}_{-2}
M_2 [M_{\odot}]	6.9 ± 1.0 $7.7^{+0.9}_{-0.8}$
q	$0.68^{+0.1}_{-0.09}$ 0.62 ± 0.06

and projected rotational velocity, $v \sin i$, and subsequently choose the best-fitting template. We rotationally broaden the spectra using the method described in (Carvalho & Johns-Krull 2023). For each template, we first minimize the χ^2 in 10 Å windows around the HeI lines (Figure 6), which are more sensitive to rotational broadening, to determine $v \sin i$ and the RV. We then refine the RV with χ^2 minimization using the full spectrum with $v \sin i$ fixed. We find the best match at $T_{\text{eff}} = 19$ kK, $\log g = 3.50$ and $Z = 0.5Z_{\odot}$. At Solar metallicity, we find the same best-matching effective temperature and surface gravity. The measured effective temperature and surface gravity are consistent with estimates from broadband Strömgren $ubvy$ photometry (Leone & Lanzafame 1997). For the best fitting template, we measure $\text{RV} = 26.5$ km/s and $v \sin i = 39$ km/s. This is the radial velocity we use when fitting the combined orbit model (Section §4). The projected rotational velocity is lower than those of B-stars found in open clusters (e.g., Santos et al. 2025), but consistent with B-stars found in the Galactic field (Huang & Gies 2008).

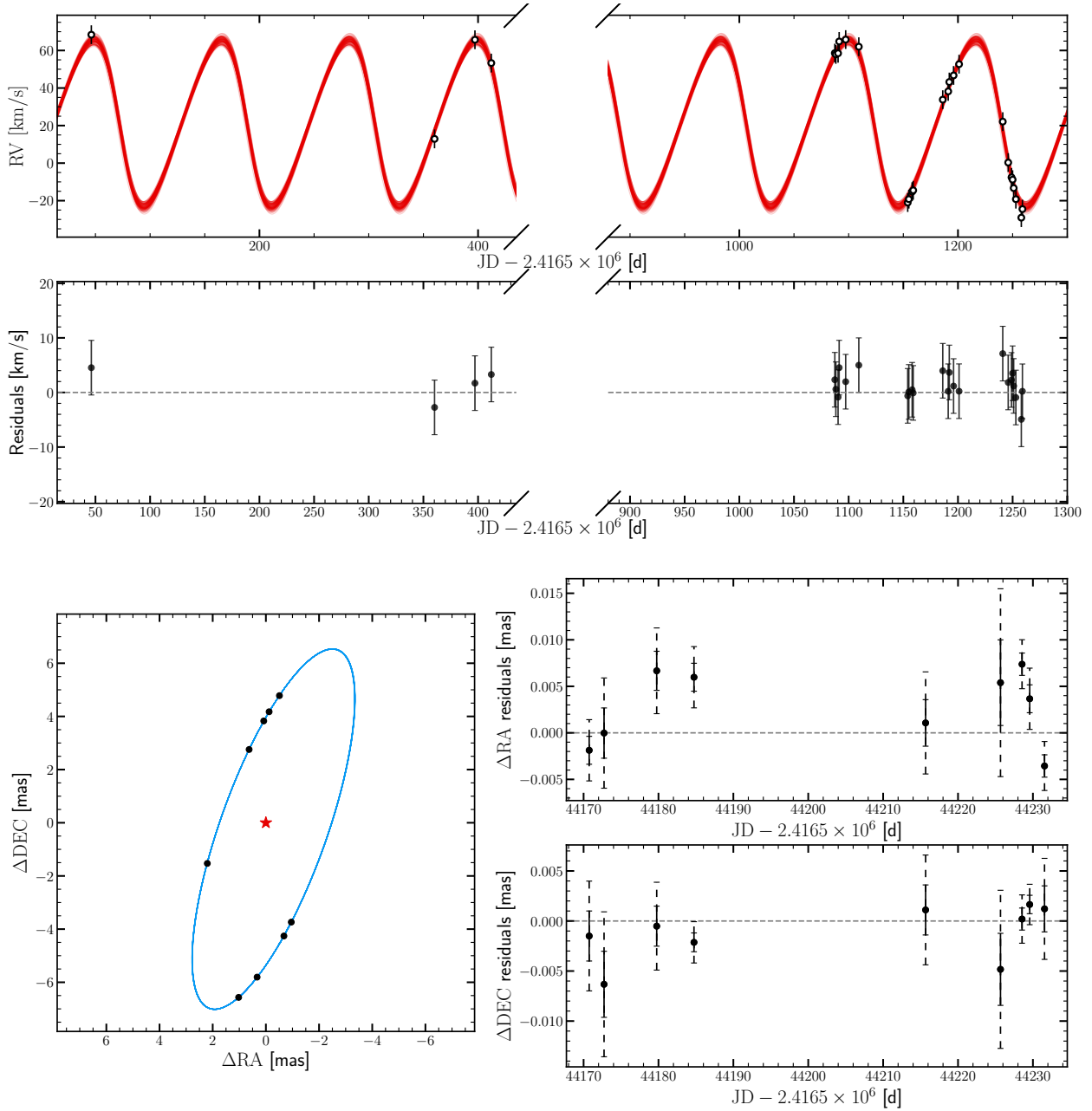


Figure 3. Top: RV orbit model and residuals. The red lines show random samples from the MCMC posteriors. Bottom left: VLTI GRAVITY astrometry measurements (black points) and random samples for the astrometric orbit model (blue). Bottom right: residuals for the astrometric orbit model. The solid errorbars give the uncertainty derived from the PMOIRE model, and the dashed errorbars report the scaled uncertainty $\sigma'_i = s_{\text{ast}}\sigma_i$.

Figure 6 shows the UVES spectrum and the synthetic spectrum of the best-fitting B-star model and marks hydrogen Balmer, He I and metal lines. The synthetic spectrum generally reproduces the observed He I and metal lines, but less accurately matches the wings of the hydrogen Balmer lines, especially at $\lambda < 4000 \text{ \AA}$. This is likely to represent an artifact of the continuum normalization procedure in areas of the spectrum dominated by the broad Balmer line wings. The Si II and O II lines between $4550 \leq \lambda \leq 4700 \text{ \AA}$ are also un-

der predicted by the best matching synthetic template, which could suggest that κ Vel is alpha-enhanced. This analysis also assumes that the spectrum is entirely dominated by the photometric primary. We evaluate this assumption in more detail in Section §6.

The spectrum is consistent with a B2V-IV star. In addition to having no He II lines, the Si II doublet at $\lambda 4129$ is clearly visible, and the C II $\lambda 4267$ line is strong. The spectrum is qualitatively similar to the B2V spectroscopic standard

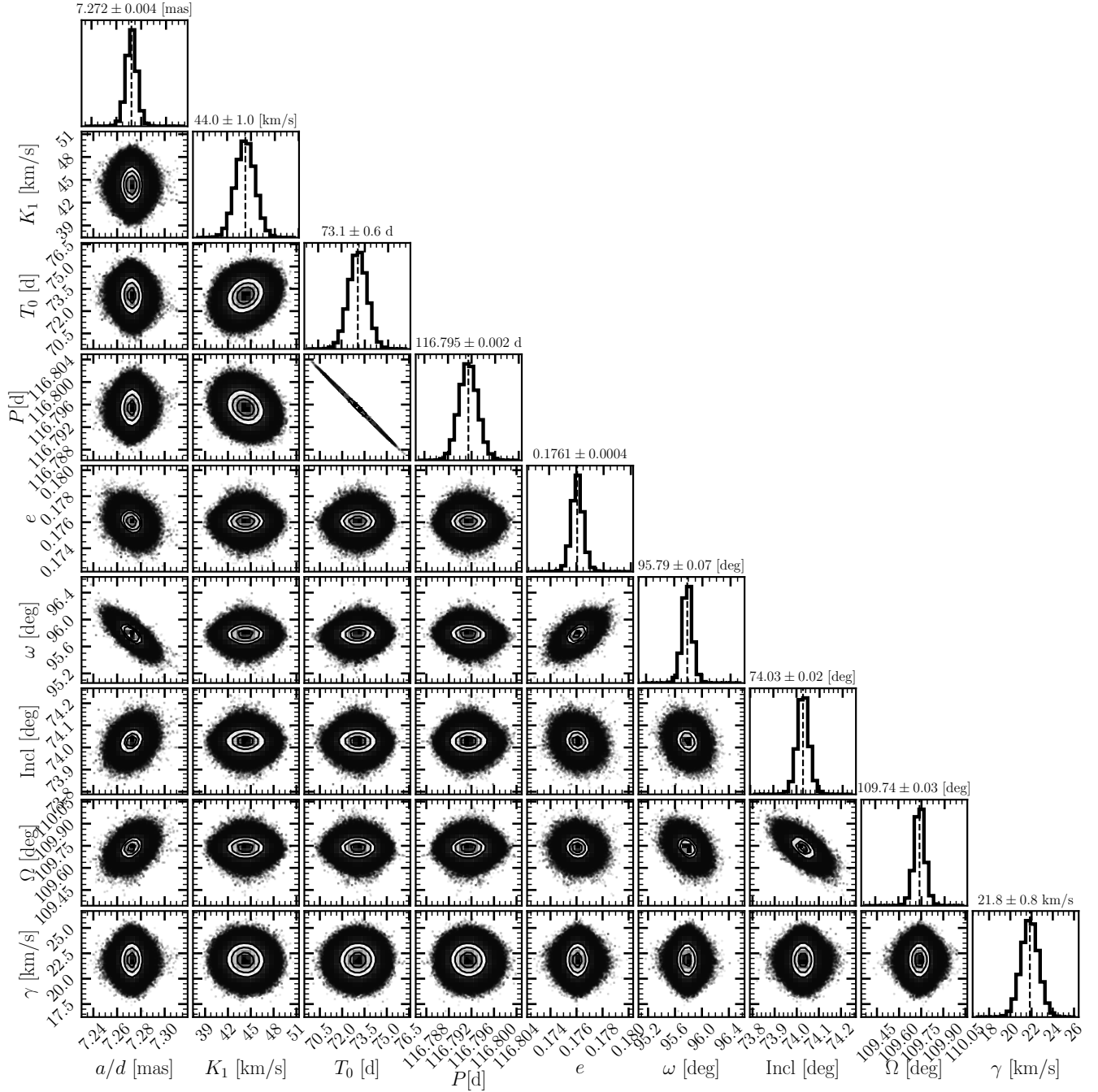


Figure 4. MCMC posteriors for orbital parameters from the simultaneous fit to the RVs and the relative astrometry.

β^2 Sco (Negueruela et al. 2024). The most notable differences between the best matching synthetic spectrum and the UVES spectrum of κ Vel are the He I lines at $\lambda\lambda 4471, 4922$. Figure 7 shows a zoom in on these absorption lines. In both cases, we observe an additional blended component in the blue wing of the primary absorption feature that is not represented by our synthetic spectra at any effective temperature, surface gravity, or metallicity. We consider two possibilities: (a) the additional component is actually the He I absorption line of

the fainter B-star companion or (b) the line list we use with Synspec does not include this blended absorption line.

For the former scenario, we find that if the component in the blue wing is the He I of the companion, the velocity difference between the components would be ~ 90 km/s. Since the UVES spectrum was taken near conjunction, we expect the velocity difference between the two components to be small. An unrealistically small mass ratio $q \lesssim 0.07$ would be needed to produce a $\Delta RV = 90$ km/s between the binary

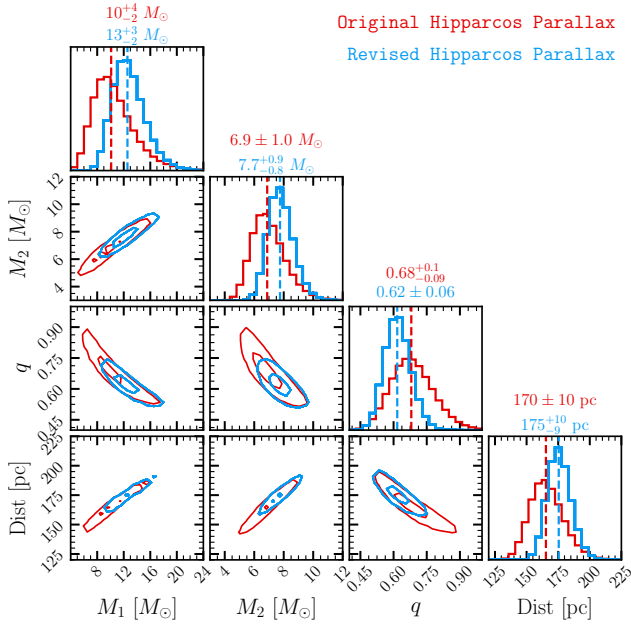


Figure 5. Mass and mass ratio posteriors computed using the orbit posteriors (Figure 4) and the original (red) and revised (blue) Hipparcos parallax measurements. Both distance measurements are consistent with the binary being a massive B+B star system.

components at the epoch of the UVES. Furthermore, we do not see evidence for blended components in the other He I lines (e.g., $\lambda 4120$, $\lambda 4143$, $\lambda 4387$) or in the C II or Mg II lines, so we reject this scenario.

While the structure in the blue wings of the He I lines at 4471\AA and 4922\AA are not predicted by our synthetic spectra, similar He I lines are found in other B and Be stars. For example, [Negueruela et al. \(2024\)](#) show that the B3V star HD 178849 has structure in the He I $\lambda 4471$ line that is not apparent in stars of the same spectral class with higher rotational velocities. Similarly, the spectrum of HD 58343, a Be2V star with $v \sin i = 43$ km/s also has a similar $\lambda 4471$ line profile ([Chauville et al. 2001](#)) which we show in Figure 7 for comparison. The most likely explanation is that the blue component of the $\lambda 4471$ comes from the forbidden transition [He I] at $\lambda 4469.96$ ([Daflon et al. 2007](#)). This is less commonly observed because it requires a high-resolution spectrum and the star to have projected rotational velocity $v \sin i \lesssim 50$ km/s (see Figure 6 of [Santos et al. 2025](#)). A forbidden [He I] line is also expected at $\lambda 4921$ ([Beauchamp & Wesemael 1998](#)), accounting for the blue wing in the He I $\lambda 4922$ profile seen in Figure 7.

6. COMPARISON TO EVOLUTIONARY TRACKS

By combining the measured binary masses and the flux ratio from the VLTI GRAVITY observations, we can estimate the evolutionary state of the binary and the spectroscopic properties of the secondary. We download precomputed evo-

lutionary tracks ([Dotter 2016](#); [Choi et al. 2016](#)) from MESA Isochrones and Stellar Tracks. For a given mass pair of M_1 and M_2 and metallicity, we interpolate their tracks onto the same age grid and calculate the K -band flux as a function of stellar age. We can then estimate the properties of both stars and the age of the system.

The measured masses are strongly dependent on the assumed parallax (Figure 5). The parallax uncertainty is large (0.3 and 0.48 mas for the original and updated measurement, respectively) and the parallax could be biased by the orbital motion by as much as 22% (Section §4). The effective temperature of the primary star measured from UVES can be used to place additional constraints on the masses of the stars. Figure 8 shows the evolution of the flux ratio of the binary system as a function of the effective temperature of the primary star assuming different parallaxes. We assume a metallicity $[\text{Fe}/\text{H}] = -0.3$ based on our template minimization results. The measured flux ratio, $\epsilon = 0.285 \pm 0.003$, implies dramatically different primary effective temperatures depending on the parallax and the derived primary mass. For example, assuming the original Hipparcos parallax $\varpi = 6.05$ mas, the flux ratio measurement implies that the photometric primary is still about halfway through its main sequence lifetime and has an effective temperature of $T_{\text{eff},1} > 25$ kK, which is much hotter than the temperature we estimate from the UVES spectrum. Figure 8 shows that the effective temperature estimate from UVES and binary flux ratio prefer a parallax of $\varpi \approx 6.5$ mas. This is $\gtrsim 1\sigma$ larger than the original Hipparcos parallax measurement and $\gtrsim 3\sigma$ larger than the revised Hipparcos parallax measurement using the reported uncertainties, but within the broader range of parallaxes acceptable if the measurement has been biased by the binary motion.

Assuming this value for the parallax, we can assess whether or not we expect to see any spectral features of the secondary in the UVES spectrum. The primary and secondary masses are $M_1 = 7.5 M_\odot$ and $M_2 = 5.9 M_\odot$, respectively. We use these masses and the orbital solution and predict that velocity difference between the primary and the secondary star at the time of the UVES observation is only $\Delta RV = 12.2$ km/s, which is not surprising given that the UVES observation was taken near conjunction. At a system age of ~ 40 Myr, which is when the K -band flux ratio matches the VLTI GRAVITY result, both stars have $T_{\text{eff}} \approx 19,000$ K, so the flux ratio is roughly the same in the K -band and in the wavelength range of the UVES spectrum. We take the synthetic spectra from the TLUSTY BSTAR2006 grid described in Section §5 and select the closest matches to the primary and secondary star. We broaden these to match the UVES resolution and apply the expected RV shifts for each component. We also rotationally broaden the spectra of both components by 40 km/s. We combine the synthetic primary and secondary spectra, weighting them such that the flux ratio is $\epsilon = 0.28$. We find

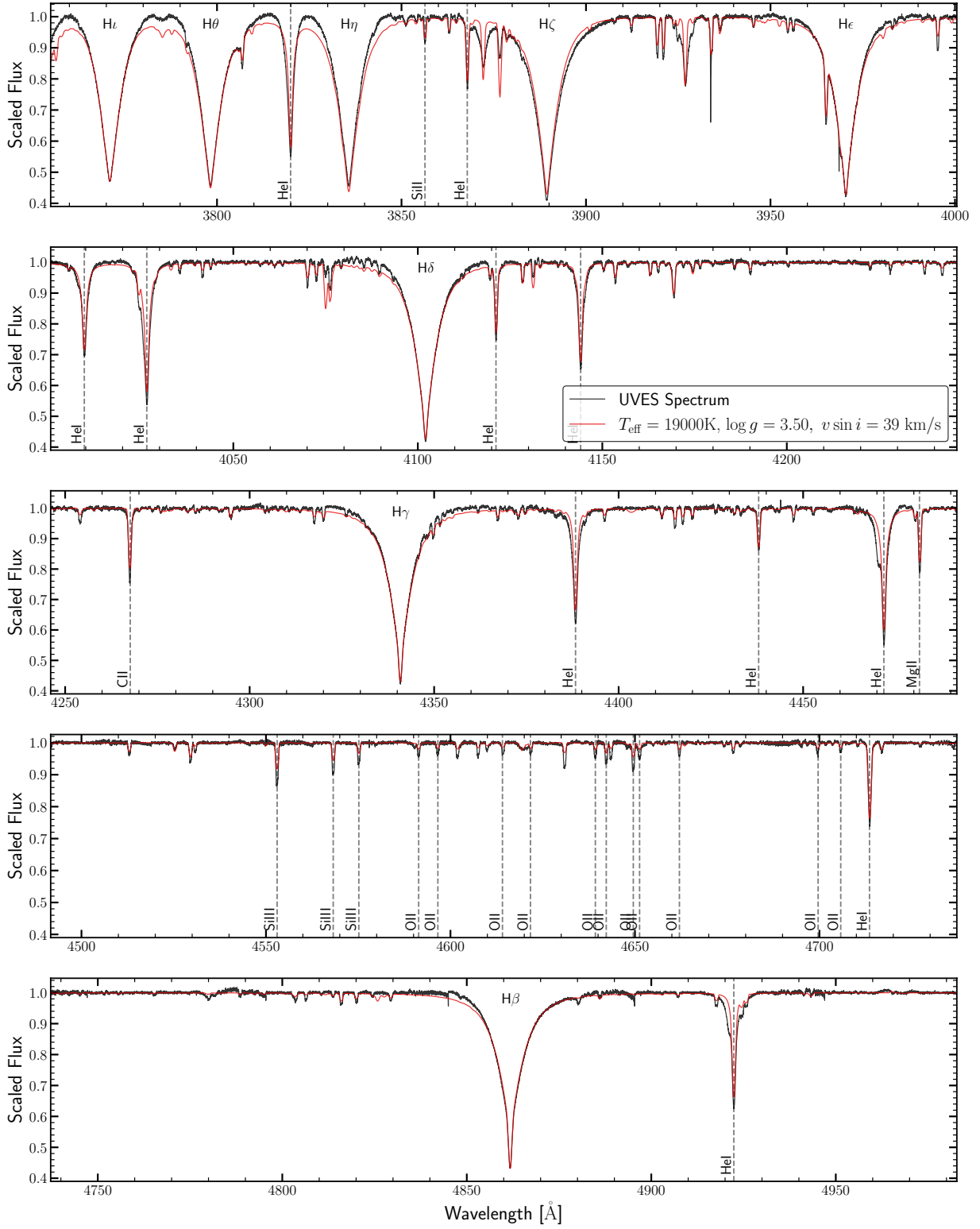


Figure 6. High-resolution UVES spectrum (black) taken as part of the EDIBLES survey (Cox et al. 2017). The red line shows the best fitting synthetic spectrum computed using TLUSTY model atmospheres and Synspec. Hydrogen, helium, and metal lines are marked using wavelengths from the NIST database (Kramida et al. 2024).

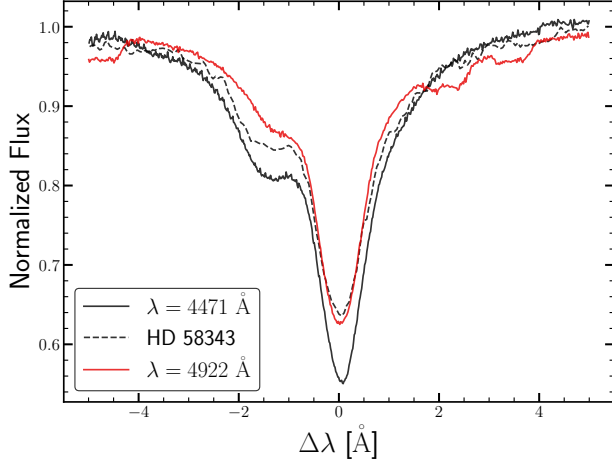


Figure 7. UVES spectrum of κ Vel showing the two He I absorption lines with asymmetric blue wings not predicted by the synthetic spectra. The $\lambda 4471$ line of the Be2V star HD 58343 from [Chauville et al. \(2001\)](#) is shown for comparison. We find that the apparent second component in the blue wings of these absorption lines is more likely from forbidden [He I] transitions rather than the stellar secondary.

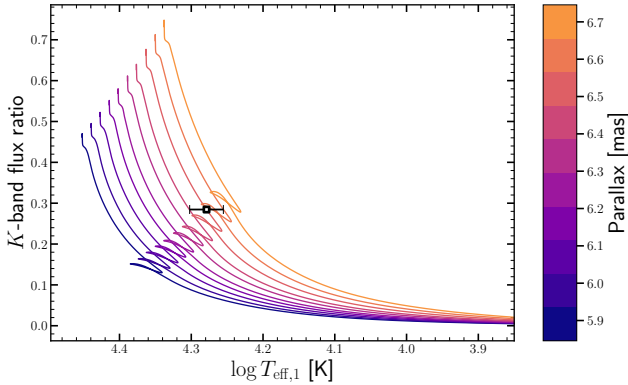


Figure 8. MIST evolutionary tracks for binary masses derived from the astrometric+RV orbit model. Since the measured masses depend on the distance to the binary, the different colors show the tracks for different parallaxes. The flux ratio from the VLTI/GRAVITY observation and the effective temperature from the UVES spectrum (black marker) are consistent with a parallax of 6.5 mas.

that the differences between the spectrum of the photometric primary and the combined binary spectrum are at the $\lesssim 2\%$ level. It is therefore unsurprising that we do not detect any signatures of the secondary in the UVES spectrum.

We also simulate the binary spectrum at RV quadrature, where we would be most likely to detect the spectroscopic signatures of the fainter companion. Figure 9 compares the synthetic spectrum of the primary at quadrature to the flux-weighted combined spectrum of both components. We find that, at quadrature, the spectrum of the primary and the combined binary spectrum differ at the $\sim 5\%$ level. The differ-

ences are most apparent in the asymmetries in the wings of the Balmer lines and split He I and metal lines.

7. DISCUSSION AND CONCLUSIONS

κ Vel is one of the brightest stars in the Southern sky and was first detected as a single lined spectroscopic binary by [Curtis \(1907\)](#). Here, we use VLTI GRAVITY to definitively determine the nature of the secondary star for the first time. To the best of our knowledge, [Daszyńska-Daszkiewicz et al. \(2017\)](#) present the only previous evidence that the companion is a massive star and not a compact object. They used BRITe photometry to characterize g -mode oscillations and found a frequencies inconsistent with the spectral type and evolutionary state of the B2V-IV photometric primary. They instead suggest that the oscillations come from a fainter, less massive B star companion.

We observed κ Vel star as part of a broader effort to identify stars with compact object companions. Given the predicted large angular separation (Figure 1) and large companion mass (Figure 2), κ Vel emerged as a promising candidate for VLTI GRAVITY observations. Although we were unambiguously able to identify the luminous secondary in the first VLTI observation, we obtained a total of nine epochs, and simultaneously fit the astrometry and RVs to model the binary orbit (Figure 3). From this model, we can predict the masses of the binary components (Figure 5 and Table 4). We find that the uncertainty in the mass measurement is primarily driven by the uncertainty in the Hipparcos parallax. It is also likely that the binary motion has biased the parallax measurement by as much as $\sim 22\%$.

Given its spectral type and magnitude, κ Vel has also been targeted by studies of diffuse interstellar bands. We use the publicly available UVES spectrum from [Cox et al. \(2017\)](#) and B-star model atmospheres to estimate the effective temperature, surface gravity, and rotational velocity of the photometric primary (Figure 6). By combining the binary flux ratio measured from VLTI GRAVITY and the effective temperature of the photometric primary, we can estimate the distance and binary masses (Figure 8).

We also use this model to estimate how the secondary star contributes to the combined spectrum. Even at RV quadrature, when the velocity difference between the two stars is largest, the synthetic binary system is expected to differ from the photometric primary at the few-percent level (Figure 9). While it may be possible to detect the subtle spectroscopic signatures of the secondary with multi-epoch high-resolution spectra and techniques like spectral disentangling (e.g., [Shenar et al. 2020](#); [Seeburger et al. 2024](#)), we detect the luminous secondary with the first VLTI GRAVITY observation. Since the orbital period and ephemeris is known from the RVs, a single VLTI observation could be used to rule out a black hole with a total observing time of ~ 1 hour,

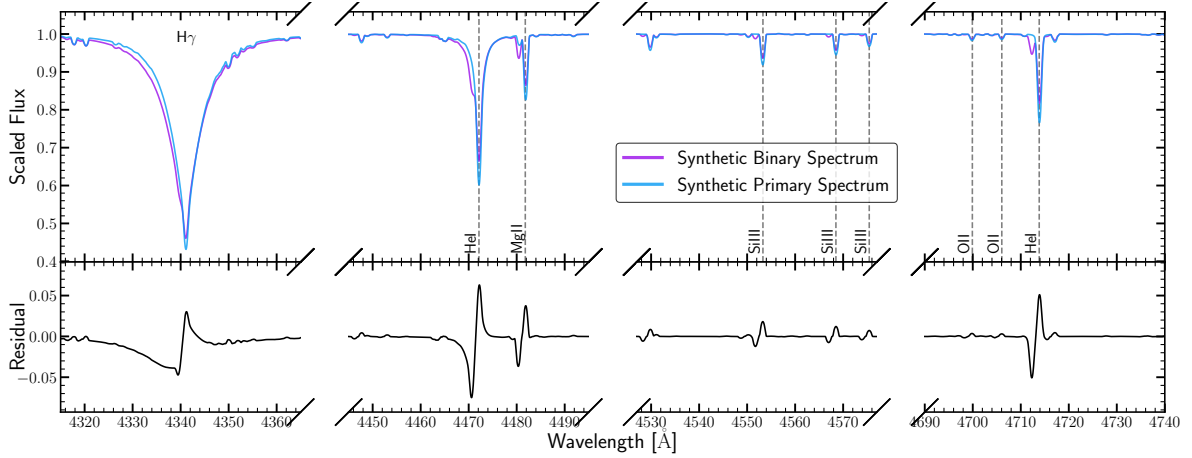


Figure 9. Synthetic spectrum of the binary system at RV quadrature, when the velocity difference between the two stars is the largest and the secondary star is mostly likely to be detected spectroscopically. The spectrum of the flux-weighted combination of the binary components (purple) differs most dramatically from that of the primary’s spectrum (blue) in the wings of the Balmer absorption lines and will also produce double-peaked He I and some metal lines, like Si II. The bottom panel shows that, at RV quadrature, the two spectra differ at the $\sim 5\%$ level. We note that the actual archival UVES spectrum (Figure 6) was taken near conjunction.

including overheads. For comparison, the single UVES spectrum shown in Figure 6 had a total observing time of 23 min, and multiple spectra ($\gtrsim 5$) taken at different orbital phases are typically needed for spectral disentangling to be effective.

7.1. Other VLTI Targets

While κ Vel does not host a black hole companion, the VLTI GRAVITY observations of this system have demonstrated how the combination of RVs and high-contrast imaging may be used to effectively and efficiently vet other candidate star+black hole binaries. As described in Section §2, we selected candidates starting from the SB9 catalog (Pourbaix et al. 2004) and the *Gaia* single-lined spectroscopic binary catalog. There are ~ 40 other binaries with minimum companion mass $M_{2,\min} > 3 M_{\odot}$ and projected angular separations > 0.5 mas that are observable with VLTI.

Table 5 reports the properties of these targets. We reject the overwhelming majority of star+black hole candidates based on archival observations, including previous spectroscopic follow-up, speckle imaging, and direct imaging. In some cases, we also use photometry from *TESS* and identify eclipses. There are four candidates from the SB9 catalog where the luminous companion has not been previously observed:

δ Gem: δ Gem is a hierarchical triple system (Tokovinin 2017). Abt (1965) report an orbital period 2238 days for the inner binary, δ Gem A. The binary mass function is $3.8 M_{\odot}$ and the photometric primary is a F2 main sequence star, so the companion would have to be $\gtrsim 6 M_{\odot}$. This orbital solution has since been questioned (Abt & Levy 1974), and the secondary in the inner binary has never been detected, including through an lunar occultation observation (Tremaine et al. 1974). δ Gem A was also observed with the Navy

Precision Optical Interferometer, but Hutter et al. (2016) do not report the detection of a companion. This may be a good candidate for high-contrast imaging or interferometry. If a luminous secondary is identified, the star can be immediately rejected as a black hole candidate. If no secondary is found, additional RVs would still be needed to confirm binary orbit.

HD 36881: HD 36881 is a chemically peculiar B9III star with an orbital period of 1862 d and a binary mass function of $0.85 M_{\odot}$. Previous high-resolution spectroscopic and VLT/NACO imaging observations have not identified the companion Schöller et al. (2010). We are observing this system in the current observing period 116 with VLTI GRAVITY.

71 Tau: 71 Tau is δ Scuti F0IV-V star with a long orbital period (5200 d) and a large binary mass function, $f(M) = 1.7 M_{\odot}$. The companion has not been previously identified with speckle interferometry (Patience et al. 1998; Mason 1996). Like δ Gem, the orbital ephemeris is uncertain (Abt & Levy 1974), and additional RVs would be needed to confirm the orbit if no companion is found with high-contrast imaging or interferometry. This star is the second brightest X-ray source in the Hyades cluster, and ultraviolet observations with the International Ultraviolet Explorer found no UV excess indicative of a hot companion (Simon & Landsman 1997). Simon & Ayres (2000) used Hubble Space Telescope UV spectra and identified an emission line source separated by $0''.12$. Simon & Ayres (2000) suggest that this signal is associated with an inner late-type binary companion that is chromospherically active that was undetected in previous interferometry observations that were taken near conjunction. This separation is consistent with the maximum angular separation we predict using *Gaia* and the SB9 orbital solution (Table 5), but Böhm-Vitense (2007) instead suggest that the

Table 5. Other candidates for VLTI/GRAVITY imaging selected from the SB9 catalog (top part of table) and *Gaia* DR3 (bottom). Archival observations confirm that most of the SB9 targets are regular stellar binaries. Most of the *Gaia* DR3 candidates are in the Hertzsprung gap and are likely luminous binaries with one red and one blue component.

Name	K_s [mag]	Period [d]	Projected Sep. [mas]	$M_{2,\min}$ [M_\odot]	Notes
X Per	5.9	3900.0	6.6	20.7	Be X-ray binary pulsar (Fortin et al. 2023)
HD 45910	4.4	232.5	1.7	8.1	B2+KIII (Cowley 1964)
χ Lup	4.0	15.3	4.1	7.2	B9.5V+ A2V (Le Bouquin et al. 2013)
δ Gem	2.6	2238.6	353.1	6.0	Uncertain RV orbit (Abt & Levy 1974)
HD 187299	3.5	1901.0	7.4	5.9	G5I + B7V (Griffin & Griffin 1979)
HD 50975	5.7	190.2	0.8	5.2	F8I + B2 (Sperauskas et al. 2014)
HD 36881	5.0	1857.0	12.7	4.3	VLTI P116 Candidate
HD 8556	4.9	5895.0	240.3	4.1	F0 + F5 (Fletcher 1973)
71 Tau	4.0	5200.0	227.4	3.9	HST UV emission lines (Simon & Ayres 2000)
HD 127208	5.1	24.6	1.0	3.8	F + Be (Dempsey et al. 1990)
ω Eri	3.7	3057.0	112.5	3.7	RV constant (Merle et al. 2024)
HD 70826	5.5	3900.0	25.7	3.5	G7III + (A+A) (Carquillat et al. 2005)
HIP 39794 (ϵ Vol)	4.7	14.2	1.2	3.2	B6IV + B8 (Veramendi & González 2014)
HIP 30891 (V723 Mon)	5.4	59.9	1.1	3.2	Stripped giant + subgiant (El-Badry et al. 2022)
HIP 51213 (45 Leo)	6.0	12658.0	146.2	3.2	Uncertain RV orbit
HIP 23900	5.3	58.3	1.4	3.1	B2V + B5-B8V (Tarasov 2016)
HIP 99853 (22 Vul)	2.9	249.1	3.3	3.0	Eclipsing G3I + B8V (Griffin et al. 1993)
Gaia DR3 5824739062379517824	8.4	1113.3	7.7	40.1	B dwarf with uncertain long-period <i>Gaia</i> orbit
Gaia DR3 5857059996952633984	9.1	155.1	0.6	8.2	Hertzsprung Gap; <i>TESS</i> eclipsing binary
Gaia DR3 3331748140308820352	9.1	225.3	0.5	5.7	Hertzsprung Gap
Gaia DR3 5971649891874353536	8.5	50.0	0.6	5.1	Hertzsprung Gap; <i>TESS</i> eclipsing binary
Gaia DR3 2021374066702077312	7.6	44.4	0.5	4.0	Hertzsprung Gap
Gaia DR3 5307540956005282560	7.7	212.7	0.9	3.6	Hertzsprung Gap; <i>TESS</i> eclipsing binary
Gaia DR3 5879279305887191552	7.7	167.7	0.6	3.4	Hertzsprung Gap
Gaia DR3 6021285355771958528	9.0	269.5	6.3	3.3	–
Gaia DR3 3179591300281505664	9.2	857.7	2.0	3.2	Hertzsprung Gap
Gaia DR3 2017710455239591424	9.0	331.7	1.1	3.2	–
Gaia DR3 6077083852882264320	8.9	897.6	2.6	3.1	Hertzsprung Gap
Gaia DR3 5335226727540945536	8.0	195.8	0.5	3.0	Hertzsprung Gap; <i>TESS</i> eclipsing binary

offset UV emission lines instead suggest that the emission line spectrum comes from material excited by a supernovae in the cluster.

45 Leo: 45 Leo is a chemically peculiar B9IV star (Loden 1983) with an uncertain long-period orbit with $f(M) = 1.1 M_\odot$ (Abt & Snowden 1973). The binary has not been resolved with speckle interferometry (Hartkopf & McAlister 1984).

Table 5 also includes the 12 sources selected from *Gaia* DR3 that are brighter than $K < 9.5$ mag, which is the magnitude limit for single-field mode observations with VLTI GRAVITY. Almost all of the targets are in the Hertzsprung gap on the color-magnitude diagram, and are likely to be binaries with an evolved red giant star and a massive main sequence star. The evolved star likely dominates the spectral

energy distribution in the wavelength range of the *Gaia* RVS (846–870 nm) so the systems are detected SB1s.

Gaia DR3 does not include the epoch RVs for the SB1 solutions, only the orbit model and covariance matrix of the posteriors, so it can be challenging to discriminate between accurate binary orbits and spurious solutions (e.g., Bashi et al. 2022). For example, the *Gaia* SB1 solution for Gaia DR3 5824739062379517824 has a very high mass function, $f(M) = 32^{+6}_{-9} M_\odot$, but the orbital period is long (> 1000 d) and is comparable to the baseline of the *Gaia* DR3 data. The photometric primary is also an early-type main sequence star with extinction-corrected $G_{BP} - G_{RP} < 0$. Such a star will likely only have broad hydrogen lines in the *Gaia* RVS spectrum, so it is possible that the solution is biased by a handful of poor RV measurements. Even though the orbit is uncer-

tain, this may still be a promising target for VLTI GRAVITY observations since a luminous companion could be identified with a small number of observations taken at different orbital phases.

While there are some candidates that are suitable for interferometric or high-contrast imaging observations, this search strategy is primarily limited by the limiting magnitude of VLTI GRAVITY at small angular separations and the number of bright stars with well-characterized long period RV orbits. For a single-field off-axis observation, the limiting magnitude is $K = 9.5$ mag using the ATs. New extreme adaptive optics instruments, such as GRAVITY+ (GRAVITY+ Collaboration 2025), will allow us to push towards fainter targets ($K \lesssim 14.5$ mag). Going forward, this strategy might best be used in conjunction with RV follow-up or *Gaia* astrometry. For example, the catalog of spectroscopic binaries in Chini et al. (2012) includes more than 80 SB1s with $K < 8.5$ mag, most of which have less than 10 RVs. By combining spectroscopic monitoring of massive stars (e.g., Mahy et al. 2022) with high-contrast imaging or interferometry with instruments such as GRAVITY, SHARK-VIS (Pedichini et al. 2024), or CHARA (ten Brummelaar et al. 2005), candidates could be vetted more efficiently than with spectroscopic follow-up alone.

The number of star+compact object candidates is expected to expand dramatically with *Gaia* Data Release 4, which is scheduled to be released in late 2026 and will include epoch astrometry and radial velocities. *Gaia* BH3 (Gaia Collaboration et al. 2024), which was discovered using pre-release *Gaia* DR4 astrometry, has already been observed with

VLTI GRAVITY to place limits on the near-infrared emission (Kervella et al. 2025). Nagarajan et al. (2025) predict that ~ 30 black holes will be detectable with *Gaia* DR4, and some of these long-period candidates will likely be suitable for high-contrast imaging or interferometric observations to confirm dark companions.

ACKNOWLEDGMENTS

Support for this work was provided by NASA through the NASA Hubble Fellowship grant HST-HF2-51588.001-A awarded by the Space Telescope Science Institute, which is operated by the Association of Universities for Research in Astronomy, Inc., for NASA, under contract NAS5-26555.

S.K. acknowledges support from an European Research Council (ERC) Consolidator Grant (Grant Agreement ID 101003096), as well as an STFC Small Award (ST/Y002695/1).

The VLTI GRAVITY observations were collected at the European Organisation for Astronomical Research in the Southern Hemisphere under ESO programme 114.274C. The UVES analysis is based on observations collected at the European Organisation for Astronomical Research in the Southern Hemisphere under ESO programme 194.C-0833. This research has made use of the SIMBAD database, operated at CDS, Strasbourg, France. This research has made use of the VizieR catalogue access tool, CDS, Strasbourg, France.

REFERENCES

- Abrams, N. S., Hundertmark, M. P. G., Khakpash, S., et al. 2025, *ApJS*, 276, 10, doi: [10.3847/1538-4365/ad91b0](https://doi.org/10.3847/1538-4365/ad91b0)
- Abt, H. A. 1965, *ApJS*, 11, 429, doi: [10.1086/190120](https://doi.org/10.1086/190120)
- Abt, H. A., & Levy, S. G. 1974, *ApJ*, 188, 291, doi: [10.1086/152716](https://doi.org/10.1086/152716)
- Abt, H. A., & Snowden, M. S. 1973, *ApJS*, 25, 137, doi: [10.1086/190265](https://doi.org/10.1086/190265)
- Anders, F., Khalatyan, A., Queiroz, A. B. A., et al. 2022, *A&A*, 658, A91, doi: [10.1051/0004-6361/202142369](https://doi.org/10.1051/0004-6361/202142369)
- Bashi, D., Shahaf, S., Mazeh, T., et al. 2022, *MNRAS*, 517, 3888, doi: [10.1093/mnras/stac2928](https://doi.org/10.1093/mnras/stac2928)
- Beauchamp, A., & Wesemael, F. 1998, *ApJ*, 496, 395, doi: [10.1086/305357](https://doi.org/10.1086/305357)
- Böhm-Vitense, E. 2007, *AJ*, 133, 1903, doi: [10.1086/512124](https://doi.org/10.1086/512124)
- Buscombe, W., & Morris, P. M. 1960, *MNRAS*, 121, 263, doi: [10.1093/mnras/121.3.263](https://doi.org/10.1093/mnras/121.3.263)
- Carquillat, J.-M., Prieur, J.-L., & Ginestet, N. 2005, *MNRAS*, 360, 718, doi: [10.1111/j.1365-2966.2005.09065.x](https://doi.org/10.1111/j.1365-2966.2005.09065.x)
- Carvalho, A., & Johns-Krull, C. M. 2023, *Research Notes of the American Astronomical Society*, 7, 91, doi: [10.3847/2515-5172/acd37e](https://doi.org/10.3847/2515-5172/acd37e)
- Chakrabarti, S., Simon, J. D., Craig, P. A., et al. 2023, *AJ*, 166, 6, doi: [10.3847/1538-3881/accf21](https://doi.org/10.3847/1538-3881/accf21)
- Chauville, J., Zorec, J., Ballereau, D., et al. 2001, *A&A*, 378, 861, doi: [10.1051/0004-6361:20011202](https://doi.org/10.1051/0004-6361:20011202)
- Chelli, A., Duvert, G., Bourgès, L., et al. 2016, *A&A*, 589, A112, doi: [10.1051/0004-6361/201527484](https://doi.org/10.1051/0004-6361/201527484)
- Chini, R., Hoffmeister, V. H., Nasser, A., Stahl, O., & Zinnecker, H. 2012, *MNRAS*, 424, 1925, doi: [10.1111/j.1365-2966.2012.21317.x](https://doi.org/10.1111/j.1365-2966.2012.21317.x)
- Choi, J., Dotter, A., Conroy, C., et al. 2016, *ApJ*, 823, 102, doi: [10.3847/0004-637X/823/2/102](https://doi.org/10.3847/0004-637X/823/2/102)
- Corral-Santana, J. M., Casares, J., Muñoz-Darias, T., et al. 2016, *A&A*, 587, A61, doi: [10.1051/0004-6361/201527130](https://doi.org/10.1051/0004-6361/201527130)
- Cowley, A. P. 1964, *ApJ*, 139, 817, doi: [10.1086/147819](https://doi.org/10.1086/147819)

- Cox, N. L. J., Cami, J., Farhang, A., et al. 2017, *A&A*, 606, A76, doi: [10.1051/0004-6361/201730912](https://doi.org/10.1051/0004-6361/201730912)
- Crawford, I. A. 1991, *A&A*, 247, 183
- . 2002, *MNRAS*, 334, L33, doi: [10.1046/j.1365-8711.2002.05730.x](https://doi.org/10.1046/j.1365-8711.2002.05730.x)
- Curtis, H. D. 1907, *ApJ*, 26, 271, doi: [10.1086/141502](https://doi.org/10.1086/141502)
- Daflon, S., Cunha, K., de Araújo, F. X., Wolff, S., & Przybilla, N. 2007, *AJ*, 134, 1570, doi: [10.1086/521707](https://doi.org/10.1086/521707)
- Daszyńska-Daszkiewicz, J., Walczak, P., Pamyatnykh, A., Jerzykiewicz, M., & Pigulski, A. 2017, in *Second BRITE-Constellation Science Conference: Small Satellites - Big Science*, ed. K. Zwintz & E. Poretti, Vol. 5, 138–144, doi: [10.48550/arXiv.1701.00961](https://doi.org/10.48550/arXiv.1701.00961)
- Dempsey, R. C., Parsons, S. B., Bopp, B. W., & Fekel, F. C. 1990, *PASP*, 102, 312, doi: [10.1086/132636](https://doi.org/10.1086/132636)
- Dotter, A. 2016, *ApJS*, 222, 8, doi: [10.3847/0067-0049/222/1/8](https://doi.org/10.3847/0067-0049/222/1/8)
- El-Badry, K., Seeburger, R., Jayasinghe, T., et al. 2022, *MNRAS*, 512, 5620, doi: [10.1093/mnras/stac815](https://doi.org/10.1093/mnras/stac815)
- El-Badry, K., Rix, H.-W., Quataert, E., et al. 2023a, *MNRAS*, 518, 1057, doi: [10.1093/mnras/stac3140](https://doi.org/10.1093/mnras/stac3140)
- El-Badry, K., Rix, H.-W., Cendes, Y., et al. 2023b, *MNRAS*, 521, 4323, doi: [10.1093/mnras/stad799](https://doi.org/10.1093/mnras/stad799)
- ESA, ed. 1997, *ESA Special Publication*, Vol. 1200, *The HIPPARCOS and TYCHO catalogues. Astrometric and photometric star catalogues derived from the ESA HIPPARCOS Space Astrometry Mission*
- Fabrizius, C., Luri, X., Arenou, F., et al. 2021, *A&A*, 649, A5, doi: [10.1051/0004-6361/202039834](https://doi.org/10.1051/0004-6361/202039834)
- Fletcher, J. M. 1973, *JRASC*, 67, 255
- Foreman-Mackey, D., Hogg, D. W., Lang, D., & Goodman, J. 2013, *PASP*, 125, 306, doi: [10.1086/670067](https://doi.org/10.1086/670067)
- Fortin, F., García, F., Simaz Bunzel, A., & Chaty, S. 2023, *A&A*, 671, A149, doi: [10.1051/0004-6361/202245236](https://doi.org/10.1051/0004-6361/202245236)
- Frost, A. J., Bodensteiner, J., Rivinius, T., et al. 2022, *A&A*, 659, L3, doi: [10.1051/0004-6361/202143004](https://doi.org/10.1051/0004-6361/202143004)
- Fruscione, A., Hawkins, I., Jelinsky, P., & Wiercigroch, A. 1994, *ApJS*, 94, 127, doi: [10.1086/192075](https://doi.org/10.1086/192075)
- Gaia Collaboration, Arenou, F., Babusiaux, C., et al. 2023, *A&A*, 674, A34, doi: [10.1051/0004-6361/202243782](https://doi.org/10.1051/0004-6361/202243782)
- Gaia Collaboration, Panuzzo, P., Mazeh, T., et al. 2024, *A&A*, 686, L2, doi: [10.1051/0004-6361/202449763](https://doi.org/10.1051/0004-6361/202449763)
- Giesers, B., Dreizler, S., Husser, T.-O., et al. 2018, *MNRAS*, 475, L15, doi: [10.1093/mnras/rlx203](https://doi.org/10.1093/mnras/rlx203)
- Gosset, E., Damerdj, Y., Morel, T., et al. 2024, *arXiv e-prints*, arXiv:2410.14372. <https://arxiv.org/abs/2410.14372>
- GRAVITY+ Collaboration. 2025, *arXiv e-prints*, arXiv:2509.21431, doi: [10.48550/arXiv.2509.21431](https://doi.org/10.48550/arXiv.2509.21431)
- GRAVITY Collaboration, Abuter, R., Accardo, M., et al. 2017, *A&A*, 602, A94, doi: [10.1051/0004-6361/201730838](https://doi.org/10.1051/0004-6361/201730838)
- Green, M. J., Ziv, Y., Rix, H.-W., et al. 2025, *A&A*, 695, A210, doi: [10.1051/0004-6361/202453271](https://doi.org/10.1051/0004-6361/202453271)
- Griffin, R., & Griffin, R. 1979, *MNRAS*, 187, 91, doi: [10.1093/mnras/187.1.91](https://doi.org/10.1093/mnras/187.1.91)
- Griffin, R. E. M., Hunsch, M., Marshall, K. P., Griffin, R. F., & Schroder, K. P. 1993, *A&A*, 274, 225
- Hartkopf, W. I., & McAlister, H. A. 1984, *PASP*, 96, 105, doi: [10.1086/131309](https://doi.org/10.1086/131309)
- Hill, J. M., Green, R. F., Ashby, D. S., et al. 2010, in *Society of Photo-Optical Instrumentation Engineers (SPIE) Conference Series*, Vol. 7733, *Ground-based and Airborne Telescopes III*, ed. L. M. Stepp, R. Gilmozzi, & H. J. Hall, 77330C, doi: [10.1117/12.856479](https://doi.org/10.1117/12.856479)
- Huang, W., & Gies, D. R. 2008, *ApJ*, 683, 1045, doi: [10.1086/590106](https://doi.org/10.1086/590106)
- Hubeny, I., & Lanz, T. 2011, *Synspec: General Spectrum Synthesis Program*, *Astrophysics Source Code Library*, record ascl:1109.022
- Hutter, D. J., Zavala, R. T., Tycner, C., et al. 2016, *ApJS*, 227, 4, doi: [10.3847/0067-0049/227/1/4](https://doi.org/10.3847/0067-0049/227/1/4)
- Jayasinghe, T., Thompson, T. A., Kochanek, C. S., et al. 2022, *MNRAS*, 516, 5945, doi: [10.1093/mnras/stac2187](https://doi.org/10.1093/mnras/stac2187)
- Jenniskens, P., Mulas, G., Porceddu, I., & Benvenuti, P. 1997, *A&A*, 327, 337
- Kalogera, V., & Webbink, R. F. 1996, *ApJ*, 458, 301, doi: [10.1086/176813](https://doi.org/10.1086/176813)
- Kervella, P., Panuzzo, P., Gallenne, A., et al. 2025, *A&A*, 695, L1, doi: [10.1051/0004-6361/202453535](https://doi.org/10.1051/0004-6361/202453535)
- Kramida, A., Yu. Ralchenko, Reader, J., & and NIST ASD Team. 2024, *NIST Atomic Spectra Database (ver. 5.12)*, [Online]. Available: <https://physics.nist.gov/asd> [2025, September 2]. National Institute of Standards and Technology, Gaithersburg, MD.
- Lam, C. Y., & Lu, J. R. 2023, *ApJ*, 955, 116, doi: [10.3847/1538-4357/aced4a](https://doi.org/10.3847/1538-4357/aced4a)
- Lam, C. Y., Lu, J. R., Udalski, A., et al. 2022, *ApJL*, 933, L23, doi: [10.3847/2041-8213/ac7442](https://doi.org/10.3847/2041-8213/ac7442)
- Lam, C. Y., Abrams, N., Andrews, J., et al. 2023, *arXiv e-prints*, arXiv:2306.12514, doi: [10.48550/arXiv.2306.12514](https://doi.org/10.48550/arXiv.2306.12514)
- Landstreet, J. D., Kupka, F., Ford, H. A., et al. 2009, *A&A*, 503, 973, doi: [10.1051/0004-6361/200912083](https://doi.org/10.1051/0004-6361/200912083)
- Lanz, T., & Hubeny, I. 2007, *ApJS*, 169, 83, doi: [10.1086/511270](https://doi.org/10.1086/511270)
- Le Bouquin, J. B., Beust, H., Duvert, G., et al. 2013, *A&A*, 551, A121, doi: [10.1051/0004-6361/201220454](https://doi.org/10.1051/0004-6361/201220454)
- Leone, F., & Lanzafame, A. C. 1997, *A&A*, 320, 893
- Levato, H. 1975, *A&AS*, 19, 91
- Loden, L. O. 1983, *A&AS*, 53, 33
- Mahy, L., Sana, H., Shenar, T., et al. 2022, *A&A*, 664, A159, doi: [10.1051/0004-6361/202243147](https://doi.org/10.1051/0004-6361/202243147)
- Mason, B. D. 1996, *AJ*, 112, 2260, doi: [10.1086/118179](https://doi.org/10.1086/118179)

- Mérand, A. 2022, in Society of Photo-Optical Instrumentation Engineers (SPIE) Conference Series, Vol. 12183, Optical and Infrared Interferometry and Imaging VIII, ed. A. Mérand, S. Sallum, & J. Sanchez-Bermudez, 121831N, doi: [10.1117/12.2626700](https://doi.org/10.1117/12.2626700)
- Merle, T., Pourbaix, D., Jorissen, A., et al. 2024, A&A, 684, A74, doi: [10.1051/0004-6361/202345918](https://doi.org/10.1051/0004-6361/202345918)
- Morris, S. L., & Naftilan, S. A. 1993, ApJ, 419, 344, doi: [10.1086/173488](https://doi.org/10.1086/173488)
- Nagarajan, P., El-Badry, K., Chawla, C., et al. 2025, PASP, 137, 044202, doi: [10.1088/1538-3873/adc839](https://doi.org/10.1088/1538-3873/adc839)
- Negueruela, I., Simón-Díaz, S., de Burgos, A., Casasbuenas, A., & Beck, P. G. 2024, A&A, 690, A176, doi: [10.1051/0004-6361/202449298](https://doi.org/10.1051/0004-6361/202449298)
- Orosz, J. A., Kuulkers, E., van der Klis, M., et al. 2001, ApJ, 555, 489, doi: [10.1086/321442](https://doi.org/10.1086/321442)
- Patience, J., Ghez, A. M., Reid, I. N., Weinberger, A. J., & Matthews, K. 1998, AJ, 115, 1972, doi: [10.1086/300321](https://doi.org/10.1086/300321)
- Pecaut, M. J., & Mamajek, E. E. 2013, ApJS, 208, 9, doi: [10.1088/0067-0049/208/1/9](https://doi.org/10.1088/0067-0049/208/1/9)
- Pedichini, F., Piazzesi, R., Viavattene, G., et al. 2022, in Society of Photo-Optical Instrumentation Engineers (SPIE) Conference Series, Vol. 12185, Adaptive Optics Systems VIII, ed. L. Schreiber, D. Schmidt, & E. Vernet, 121856Q, doi: [10.1117/12.2629244](https://doi.org/10.1117/12.2629244)
- Pedichini, F., Piazzesi, R., Causi, G. L., et al. 2024, in International Society for Optics and Photonics, Vol. 13097, Adaptive Optics Systems IX, ed. K. J. Jackson, D. Schmidt, & E. Vernet (SPIE), 130970A, doi: [10.1117/12.3018651](https://doi.org/10.1117/12.3018651)
- Pourbaix, D., Tokovinin, A. A., Batten, A. H., et al. 2004, A&A, 424, 727, doi: [10.1051/0004-6361:20041213](https://doi.org/10.1051/0004-6361:20041213)
- Price-Whelan, A. M., Hogg, D. W., Foreman-Mackey, D., & Rix, H.-W. 2017, ApJ, 837, 20, doi: [10.3847/1538-4357/aa5e50](https://doi.org/10.3847/1538-4357/aa5e50)
- Rowan, D. M., Stanek, K. Z., Jayasinghe, T., et al. 2021, MNRAS, 507, 104, doi: [10.1093/mnras/stab2126](https://doi.org/10.1093/mnras/stab2126)
- Rowan, D. M., Thompson, T. A., Kochanek, C. S., et al. 2025, ApJ, 981, 94, doi: [10.3847/1538-4357/adad6e](https://doi.org/10.3847/1538-4357/adad6e)
- Russell, T. D., Del Santo, M., Marino, A., et al. 2022, MNRAS, 513, 6196, doi: [10.1093/mnras/stac1332](https://doi.org/10.1093/mnras/stac1332)
- Santos, W., Daflon, S., Silva, J. V. S., et al. 2025, MNRAS, 541, 1449, doi: [10.1093/mnras/staf912](https://doi.org/10.1093/mnras/staf912)
- Schöller, M., Correia, S., Hubrig, S., & Ageorges, N. 2010, A&A, 522, A85, doi: [10.1051/0004-6361/201014246](https://doi.org/10.1051/0004-6361/201014246)
- Seeburger, R., Rix, H.-W., El-Badry, K., Xiang, M., & Fouesneau, M. 2024, MNRAS, 530, 1935, doi: [10.1093/mnras/stae982](https://doi.org/10.1093/mnras/stae982)
- Shenar, T., Bodensteiner, J., Abdul-Masih, M., et al. 2020, A&A, 639, L6, doi: [10.1051/0004-6361/202038275](https://doi.org/10.1051/0004-6361/202038275)
- Shenar, T., Sana, H., Mahy, L., et al. 2022, Nature Astronomy, 6, 1085, doi: [10.1038/s41550-022-01730-y](https://doi.org/10.1038/s41550-022-01730-y)
- Simon, T., & Ayres, T. R. 2000, ApJ, 539, 325, doi: [10.1086/309228](https://doi.org/10.1086/309228)
- Simon, T., & Landsman, W. B. 1997, ApJ, 484, 360, doi: [10.1086/304321](https://doi.org/10.1086/304321)
- Smith, K. T., Fossey, S. J., Cordiner, M. A., et al. 2013, MNRAS, 429, 939, doi: [10.1093/mnras/sts310](https://doi.org/10.1093/mnras/sts310)
- Sperauskas, J., Zács, L., Raudeliūnas, S., Musaev, F., & Puzin, V. 2014, A&A, 570, A3, doi: [10.1051/0004-6361/201322888](https://doi.org/10.1051/0004-6361/201322888)
- Tanikawa, A., Hattori, K., Kawanaka, N., et al. 2023, ApJ, 946, 79, doi: [10.3847/1538-4357/acbf36](https://doi.org/10.3847/1538-4357/acbf36)
- Tarasov, A. E. 2016, Astronomy Letters, 42, 598, doi: [10.1134/S1063773716080077](https://doi.org/10.1134/S1063773716080077)
- Tauris, T. M., & van den Heuvel, E. P. J. 2006, in Compact stellar X-ray sources, ed. W. H. G. Lewin & M. van der Klis, Vol. 39 (Cambridge University Press), 623–665, doi: [10.48550/arXiv.astro-ph/0303456](https://doi.org/10.48550/arXiv.astro-ph/0303456)
- ten Brummelaar, T. A., McAlister, H. A., Ridgway, S. T., et al. 2005, ApJ, 628, 453, doi: [10.1086/430729](https://doi.org/10.1086/430729)
- The LIGO Scientific Collaboration, the Virgo Collaboration, & the KAGRA Collaboration. 2025a, arXiv e-prints, arXiv:2508.18083, doi: [10.48550/arXiv.2508.18083](https://doi.org/10.48550/arXiv.2508.18083)
- The LIGO Scientific Collaboration, the Virgo Collaboration, the KAGRA Collaboration, et al. 2025b, arXiv e-prints, arXiv:2508.18082, doi: [10.48550/arXiv.2508.18082](https://doi.org/10.48550/arXiv.2508.18082)
- Tokovinin, A. 2017, ApJ, 844, 103, doi: [10.3847/1538-4357/aa7746](https://doi.org/10.3847/1538-4357/aa7746)
- Torres, M. A. P., Casares, J., Jiménez-Ibarra, F., et al. 2020, ApJL, 893, L37, doi: [10.3847/2041-8213/ab863a](https://doi.org/10.3847/2041-8213/ab863a)
- Tremaine, S. D., Groth, E. J., & Nelson, M. R. 1974, AJ, 79, 649, doi: [10.1086/111590](https://doi.org/10.1086/111590)
- Trimble, V. L., & Thorne, K. S. 1969, ApJ, 156, 1013, doi: [10.1086/150032](https://doi.org/10.1086/150032)
- van Leeuwen, F. 2007, A&A, 474, 653, doi: [10.1051/0004-6361:20078357](https://doi.org/10.1051/0004-6361:20078357)
- Veramendi, M. E., & González, J. F. 2014, A&A, 567, A35, doi: [10.1051/0004-6361/201423736](https://doi.org/10.1051/0004-6361/201423736)
- Wright, W. H. 1905, ApJ, 21, 371, doi: [10.1086/141223](https://doi.org/10.1086/141223)